Original Research Article

Opto-Electrical Characterization of SnO_2 Semiconductor Based Thin Layer for the Fabrication of Innovative Diode

Mostefa Benhaliliba*

Film Device Fabrication-Characterization and Application FDFCA Research Group USTOMB, 31130, Oran, Algeria

Use yor device to scan and read the article online

Citation M. Benhaliliba. Opto-electrical Characterization of SnO_2 Semiconductor Based Thin Layer for the Fabrication of Innovative Diode. *J. Eng. Ind. Res.* **2025**, 6 (1):1-18.

https://doi.org/10.22034/jeires.2022.1.8

Article info:
Submitted: 2025-01-14
Revised: 2025-02-04
Accepted: 2025-02-22
ID: JEIRES-2501-1150

Keywords:
Crystalline structure; Transmittance; Nanostructures; Current-voltage characteristics; In-doped SnO_2; Ideality factor.

ABSTRACT

This study focuses on the thin film and related device based on indium tin oxide (SnO_2). It is produced onto glass and n-type silicon by spray pyrolysis and thermal evaporation processes. The structural, optical, dielectric, and surface properties of In-doped SnO_2 layers are investigated, and important parameters have been determined. A polycrystalline structure and a main orientation along (200) are confirmed by X-ray patterns. UV-Vis measurements of Indium-doped SnO_2 layers show a transmittance peak of 95% and 97% in the visible band. A wide optical band gap E_g of 4.06 and 4.13 eV is recorded and SnO_2 nanostructures have been revealed. The electrical conductivity σ(T) profile of SnO_2 film is reducing as 1000/T values are increasing. An evidence of dark-light conditions on the I-V characteristics of our diode based on In-doped SnO_2 is confirmed. Effect of In-doping level on the parameters extracted from I-V characteristics is emphasized. The effect of light on the diode parameters, such as ideality factor, saturation current, and photocurrent, is observed, which gives it the possibility of being used as a photodiode.

Introduction

Wide band gap semiconductor (SnO_2) with high infrared reflectivity, high transparency in the visible, wide bandgap of 3 eV, and high excitonic energy of 130 meV is among the attracted wide band gap semiconductors [1]. These materials are employed in various products due to their interesting properties, including transparent electrodes for displays, semiconductor technologies, gas sensors, heating components, and static surfaces [2]. Some elements are used as dopants in order to improve SnO_2 properties like Al, Fe, Sb, La, F, Gd, Pd, and Pt [1-9]. Gd doped-SnO_2 nanocrystals are previously produced [10]. Spray pyrolysis is a common technique since it is simple, inexpensive, unobtrusive, and environmentally friendly. In this context, we focused on the effect of indium doping, with various indium concentrations, on

*Corresponding Author: Mostefa Benhaliliba (mbenhaliliba@gmail.com)

the ultrasonic sprayed SnO_2 layers. Investigated behaviors including structural, morphological, optical and electrical are studied. Spray pyrolysis is previously used to create the transparent p-n junction diode with a p-SnO/n-SnO_2 composition [11]. The SnO_2: Fe/p-Si heterojunction tunneling transport investigation is mentioned before [3]. SnO_2 meets applications for photovoltaic cells [12], sensors [13-14], transparent conductive coating in luminescent devices are previously mentioned [15-16]. A technique to enhance the UV photo-response characteristics of SnO_2/p-Si based heterostructures using hydrothermally produced nanorods is presented [17]. Researchers [18] have mentioned a previous study on In-doped SnO_2 thin layer preparation using the sol-gel method. According to reports, thin films of SnO_2 that are pure and 15 and 30 Indium-doped show high transparency in the VIS and IR bands. SnO_2/boron-doped diamond heterojunction photodiodes fabricated by RF magnetron sputtering are mentioned previously. Furthermore, Zener diode is studied as ported by Xue *et al.* [19]. From the characteristics of the current voltage (I-V) the electronic parameters, ideal factor, effective barrier, flat band barrier height, series resistance, and saturation current density of the diodes are deduced. Under both low- and high-light conditions, the photocurrent and photoresistance are calculated. This study involves the fabrication of 4, 6, and 8 nm indium-doped SnO_2 thin layers and elated diodes. It is investigated how illumination and frequency affect the electrical characteristics of a junction based on SnO_2. In addition, the influence of light on current-voltage and frequency on capacitance-voltage characteristics are taken into account. Wide band gap diodes have been the subject of numerous studies, but none have examined the impact of indium in varying concentrations on electrical and optical properties. Up to our best knowledge rare are works mentioned on both SnO_2 thin films and diode and no studies reported on In-doped effect on structural, optical and I-V measurements in both dark and light conditions.

Experimental

In-doped Tin oxide thin films were produced via a simple and costless ultrasonic spray pyrolysis technique. The precursor was 0.1 M of $SnCl_2$, $2H_2O$ diluted in methanol during 5 min at 300 °C followed by insertion of indium (3+) chloride ($InCl_3$) as a doping source. The doping ratio In /Sn are 4, 6, and 8 % in the solution. A thermal evaporation technique under vacuum at 4.5 $x10^{-5}$ Torr was used to deposit a 120 nm thick gold contact. Using SEM inspection, the films average thickness was found as 2 µm. Structural study of SnO_2 films was achieved by Rigaku X-ray diffractometer; model DMAX 2200, having a copper anticathode (Cu K_α, 1.54Å in the range of 2θ between 20º and 70º). A Shimadzu UV-3600 PC double beam UV-VIS-NIR spectrometer was used to record the UV-VIS-NIR transmittance spectra of the SnO_2 films made at various indium concentrations. An electrometer made by Keithley, model 6517A, was used to gauge the films' electrical conductivity. Average thickness of films was about 2µm. As a result, a diode made of Ag/SnO_2/nSi/Au was produced and described. A source meter, LCR HiTESTER Hioki 3532-50 served to do the electrical measurements. A 200 W lamp was used to evaluate current voltage characteristics in the 20-100 mW/cm^2 by step 20 intensity range first in the dark, and then in light. The applied frequency was in the range of 100 to 500 Hz, while the voltage was in the range of -5 to 5 V.

Results and Discussion

X- rays pattern analysis

The films reveal a polycrystalline structure, rise preferentially in the direction (200), as displayed in Figure 1. The intensity of (200) peak augments with level doping while up to 4%, the intensity declines but 8% In-doped case demonstrates lowest peak intensity. It is observed also (111), (110), and (220) orientations with different intensities, as seen in Figure 1.

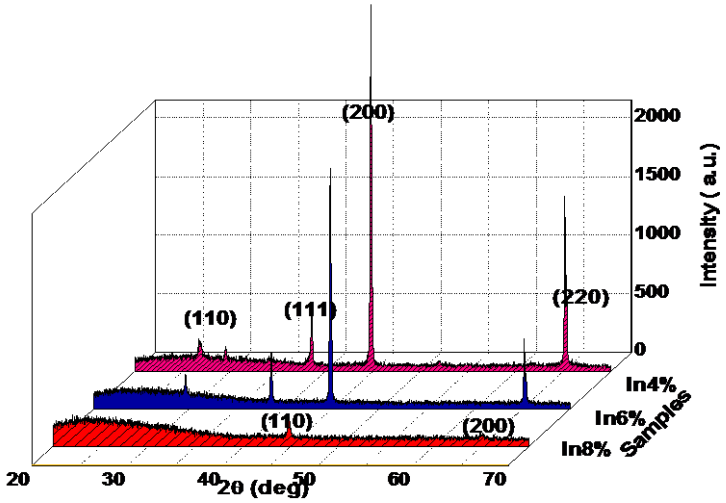

Figure 1: X-ray pattern analysis of 4, 6, and 8% In-doped SnO_2 layers.

Table 1: Structural parameters of In-doped thin layers

In Level doping (%)	2θ (°)	d(hkl) (Å)	Grain size (Å)	FWHM (°)	Direction
4	26.76	3.3287	196	0.428	(110)
	38.54	2.3341	406	0.230	(111)
	44.78	2.0223	491	0.202	(200)
	65.122	1.4313	448	0.233	(220)
6	38.6	2.3306	453	0.211	(111)
	44.839	2.0197	462	0.211	(200)
	65.181	1.4301	444	0.235	(220)
8	44.76	2.0231	289	0.314	(110)
	65.21	1.4313	174	0.552	(200)

Table 2: Textural parameter, rain size, and lattice parameters, unit cell volume of fabricated films

Level doping	TC	Grains size (200) (Å)	a(Å)	c(Å)	Volume (Å^3)
4	0.84	491	4.044	4.038	66.06
6	0.84	462	4.039	4.05	66.23
8	0.51	174	-	-	-

Table 3. Comparison of In-doped SnO_2 films grown by several routes in terms of structural, optical, and electrical characteristics

Growth route	Crystal size (nm)	Optical band gap (eV)	Max of T (%)/ρ (Ωxcm)	Ref.
Spray pyrolysis	3.4	3.96 for In-doped SnO_2	~82	[51]
Ultrasonic spray pyrolysis	17- 64	4.1	75% /10^4–10^7	[52]
Co-precipitation Method	-	3.18 - 3.11	~85	[53]
Sol-gel	4.81 - 6.8	3-4	95/ 6.08 × 10^{-3}	[18]

It is displayed a shift peak to the higher angle 2θ. A polycrystalline tetragonal rutile structure synthesized by the spin coating method and indexed diffraction peaks (110), (101), (200), (211), (220), (310), and (301) of Sm^{3+} doped SnO_2 are located according to JCPDS card no 41–1445 as mentioned previously [20]. Location of peak, d(hkl) interlayer distance, grain size, FWHM, and directions of In-doped thin layers are summarized in Table 1.

The typical peaks of Sb-doped SnO_2 thin films produced by a sol-gel spin coating process were found at 26.61°, 33.89°, 38.96°, and 51.78°, corresponding to the planes (110), (101), (111), and (211), respectively, indicating that cassiterite tetragonal crystal structure was seen in all samples [21]. It was reported that indium (In^{3+}), aluminum (Al^{3+}), gallium (Ga^{3+}), and boron (B^{3+})-doped SnO_2 lattice improve its structural, optical, and electrical properties [18,22-23]. Al^{3+} was well-known among metal due to its smaller radius (0.54) than Sn^{4+} (0.71). Our results were in well-agreement with those cited before. The crystallite size In-doped SnO_2 films was considered by well-known Scherer's expression [18]. The lattice constants a and c were determined from the X-ray patterns. According to (200) direction, the lattice parameters (Å) of SnO_2 were found to be a = 4.046 and c= 4.049, c/a ~ 1.0007 but by JCPDS-41-1445 identification, were of: a = b = 4.737, and c = 3.185 [24]. Textural parameter, rain size, and lattice parameters, unit cell volume of fabricated films are listed in Table 2.

Transmittance profile

Understanding a material's optical constants is typically very important for the design and study of materials to be used in optoelectronics. Furthermore, optical measurements are often used to describe the composition and quality of the materials. The transmittance spectrum can be used to determine optical constants such the dielectric constant, refractive index, and absorption coefficient. In order to compare transparency of In: SnO_2 films within 4-8% indium doping level, the samples are produced and analyzed. Optical transparency of films based SnO_2 layer is plotted in Figure 2. An increment of transmittance from UV band to a top of 87 % (at ~367 nm) at UV near band edge is observed as indicated by arrow in Figure 2.

Our findings are in well agreements with those of literature. Indium-doped SnO_2 recording peak points of 95% and 97% in the visible band, and 87% towards the edge of the UV band as cited prior [18]. SnO_2 thin films exhibit intense transparency in visible and infrared ranges and Fe cation reduces it slightly as reported by Ben Haj Othmen et al. [3]. Using Tauc's plot (not shown here), optical bandgap (E_g) is found to be 4.09, 4.07 and 4.11 eV respectively for 4%, 6% and 8% In-doped SnO_2 films. The transmittance falls very sharply near the UV range due to the onset of fundamental absorption as shaped in Figure 2. In literature, similar trends are found as cited by Chayoukhi et al. for 2,4 and 6% Co-doped SnO_2 layers produced by spray pyrolysis route. A highest transmittance point of 85% inside IR band and a large bandap around 4 eV are recorded for Co-doped SnO_2 layers [25]. Bandap around 3.4-3.8 eV are mentioned by Kajal et al. for SnO_2 films deposited onto FTO substrate at 400 °C via the pulsed laser deposition (PLD) route [26]. Pure and Al-doped SnO_2 thin films were grown using sol-gel spin-coating process, display a bandgap of 3.8 eV as a result of Al cation insertion in SnO_2 lattice [27].

Transmittance of the films against wavelength within 300-800 nm range describes a growth from UV band to 87% in UV range (at 365 nm). 4% In shows a slight increase with respect to 6 and 8 % In doped cases. Discrepancy might due to value of layer thickness. Additionally, the absorption edge of samples is recorded in the 300-355 nm wavelength band [28]. The variation in the absorption coefficient as a function of incident photon energy for allowed direct transitions is given by Tauc's formula [29],

$$(v\hbar\alpha)^2=hv-E_g \quad (1)$$

Where α is the absorption coefficient, h is Planck's constant, ν is the frequency, and E_g is the band gap energy. The absorption coefficient α is obtained from Beer's law,

$$I=I_o e^{-\alpha x} \quad (2)$$

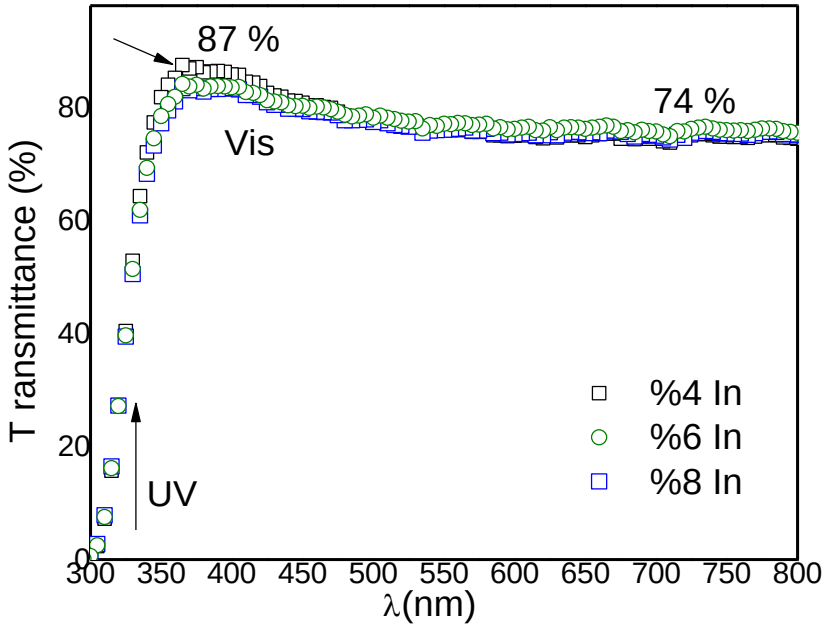

Figure 2: Transmittance variation versus wavelength of In-doped SnO_2 films.

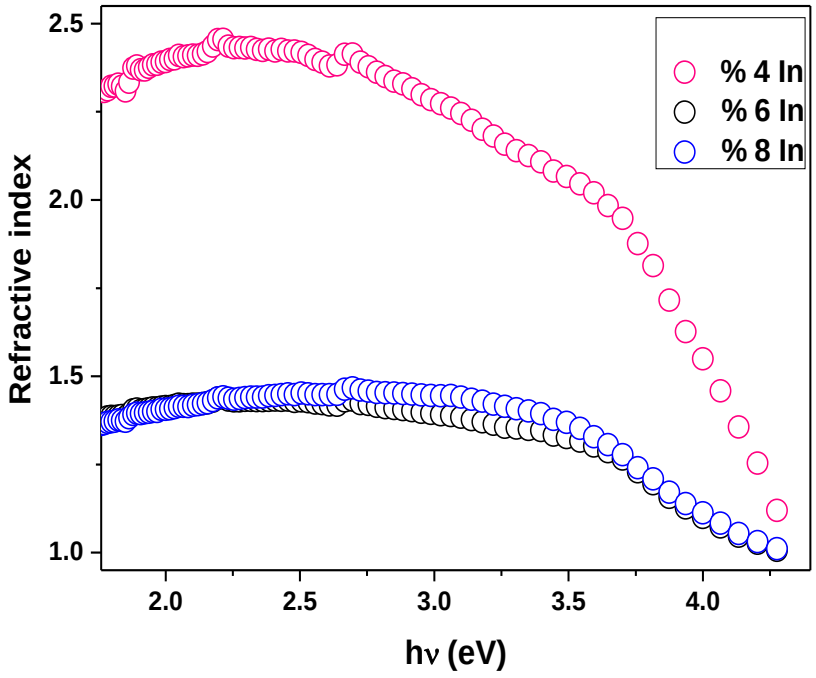

Figure 3: Description of refractive index of In-doped SnO_2 versus incident photon energy.

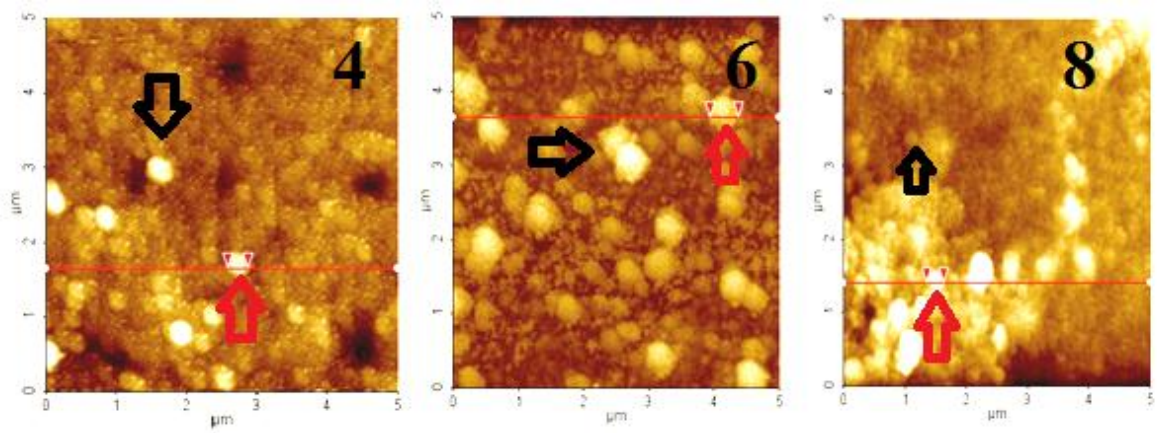

Figure 4: 2D-scanned AFM pictures of 4, 6, and 8% In-doped SnO_2 films.

Table 4: AFM parameter, RMS, E_g, and refractive index values

Indium doped SnO_2 sample (%)	**4**	**6**	**8**
Particle size by AFM (nm)	295	434	278
RMS Roughness (nm)	4.955	19.572	24.100
E_g (eV)	4.06	4.08	4.10
n (λ=550 nm)	2.48	1.40	1.42

Where, α is absorption coefficient and *x* is the thickness of the measured sample. Absorption coefficient α, optical band gap E_g, refractive index n and thickness of the films are evaluated from the transmittance/absorption spectra. From $(\alpha h\nu)^2$ plot vs. photon energy hν (eV) (not shown here) and using extrapolation of the linear part which intercepts the energy axis the value of E_g is then determined. The data of optical band gap E_g comprises inside 4.06 and 4.13 eV, as listed in Table 4.

The normal incidence reflectivity R in terms of refractive index expresses as [30]:

$$R=\frac{(n-1)^2+k^2}{(n+1)^2+k^2} \quad (1)$$

The shape of refractive index versus photon energy is shown in Figure 3 within the 1.5-4.5 eV range. It is observed that refractive index is energy dependent, as seen in Figure 3, recoding a highest value of 2.5 for 4%In doped inside visible range. Wide band gap of our films is also reported literature even the deposition route is different like In- doped SnO_2 produced by sol-gel, [18], a value of 4 eV is recorded by Kamarulzaman *et al.* for SnO_2 nanomaterials made by a self-propagating combustion process [31]. It is noted that rutile SnO_2 nanoparticles made by co-precipitation technique display a band gap of 3.6 eV as mentioned by Mohanta *et al.* [32]. Nanorods of SnO_2, ZnO, and SnO_2/ZnO composites are fabricated via the hydrothermal process. Band gap is included in 2.78-3.68 eV range. Besides such found findings of SnO_2/ZnO composite meet the optoelectronic and gas sensing device applications [33]. Table 3 indicates comparison of In-doped SnO_2 films grown by several routes in terms of structural, optical, and electrical characteristics. Semi-log curve of absorption versus photon energy (not shown here) is considered. Urbach energy Eu is determined via following equation [34]:

$$E_u = \frac{h_v - E_g}{\ln\left(\frac{\propto}{\propto_o}\right)} \quad (2)$$

Based on optical properties in particular lnα versus hν plotting, Urbach energy (Eu) values record 200 meV, 210 meV and 252 meV, respectively, for 4, 6, and 8% In-doped samples.

2D-scanned AFM pictures analysis

In semiconductor oxide thin films, the optical and electrical properties are managed by surface roughness and morphology as cited before [20]. The atomic force microscope (AFM) observation is shown in Figure 4. The following images show that all coated films are dense and homogeneously formed on the substrate, with no cluster formation. Furthermore, the grains are well distinct and spherical in structure, with no cracks. Due to the doping level, the surface is full of aggregates assembled in complete surface brilliant and less bright with various sizes ranging from 200 to 400 nm. Similar nanostructures of SnO_2:Ni/Cu are observed in work of Lolly Maria Jose *et al.* [35]. The grain size and RMS roughness of the Er-doped SnO_2 films are determined using AFM measurements, and the film surface had a saw-tooth structure as cited before [36]. The Rms parameter is calculated by Equation (3) [37]:

$$R_{rm_5} = \frac{\sum_1^n (z_i - \bar{z})^2}{N} \quad (3)$$

Where, Z_i represents the value of each point, $\overline{Z}$ is the average of the Z values and N is the number of points. 2D-AFM scanned pictures display the grains smoothness about 25.5 nm recording diverse sizes and nanosphere and nano-hexagon forms with diverse diameters and configurations, as shown in Figure 3. According to the two-dimensional profiles, the texture of the 908 nm film appeared more granular than that of the 373 nm SnO_2 film, whose microscopic grains appeared significantly smoother [38]. Size values and optical measurements as a result of In-doping level are gathered in Table 4. Nanostructures are also revealed by SEM observation in some TCO like TiO_2 and ZnO as reported previously [39-40]. Furthermore nanoparticle of meta-oxide on carbon nanotubes are occurred as mentioned previously [41].

Electrical conductivity dependency on temperature

Figure 5 illustrates how the profile of conductivity σ(T) is reducing as 1000/T values rise at 290-500 K.

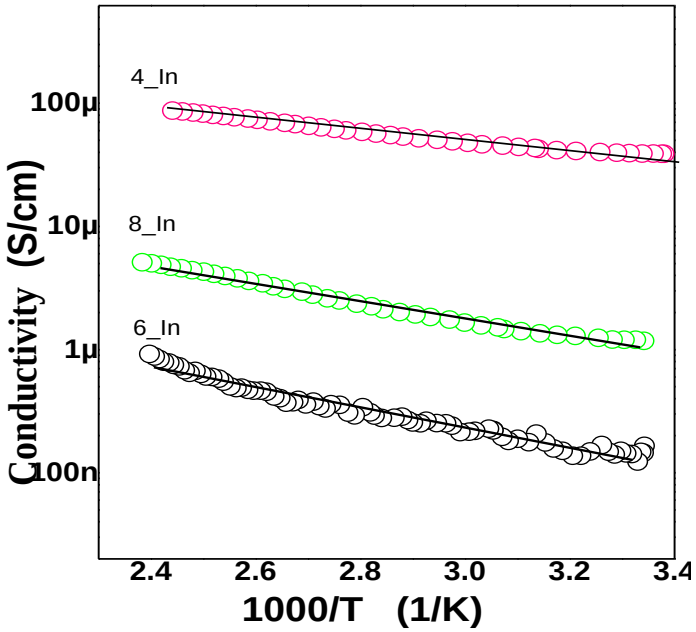

Figure 5: Variation of electrical conductivity of In-doped SnO_2layers in terms of 1000/T.

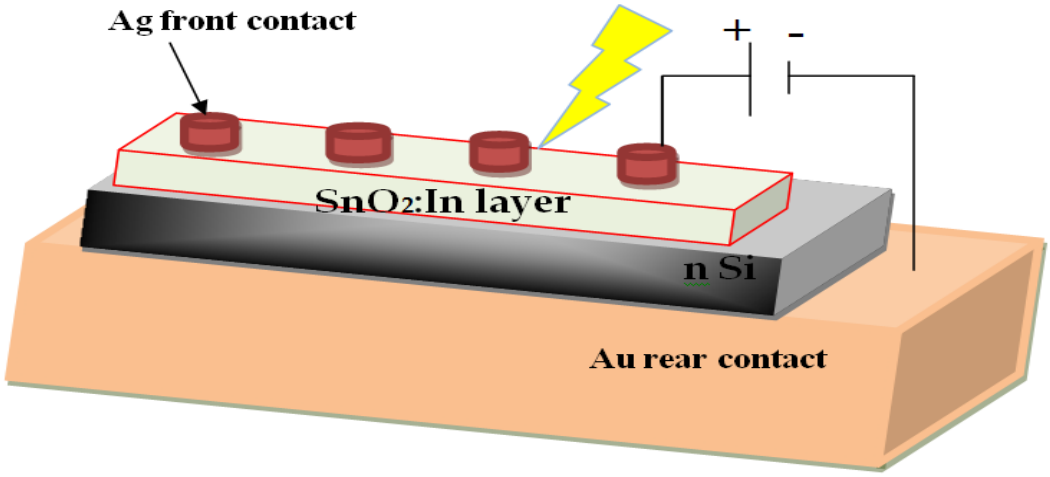

Figure 6: The measuring setup and the Ag/SnO_2:In/Si/Au junction structure arrangement.

Due to In-doping rate, σ(T) values range from 100 nS/cm to 100 S/cm whereas the 6 and 8 In-doped SnO_2 layers are less conductive, the 4 In-doped layers is more conductive.

The films display semiconducting activity, and the semi-log figure displays one conduction mechanism followed by a slope. From 100 S/cm for 4% In-doped film to 100 nS/cm for 6% In-doped one, electrical conductivity decreases significantly. The critical device parameter E is then derived from the slope as indicated by ln $(\sigma/\sigma_0)=-\Delta E/k_BT$. The electrical conductivity dependency on temperature T is expressed by [42];

$$\sigma = \sigma_0 \exp\left(-\frac{\Delta E}{kT}\right) \quad (4)$$

Where, σ_0 is the conductivity at 1/T = 0, E is the thermal activation energy, and k = 8.62 10^{-5} eV is the Boltzmann constant. It is early mentioned that SnO_2/FTO produced by PLD exhibited a conductivity of 1.47 S/cm and a bulk concentration of 2.6x10^{21} cm^3 [26]. As reported in [27], a resistivity within the range of 10^{-3}-10^{-4} Ωxcm was found in Al-doped SnO_2 films. According to prior research, SnO_2 nanostructures have a conductivity of 2-12 μS/cm [31]. Plots of ln(σ) vs. temperature of p–n homojunction diode-based Ga-doped SnO_2 determine the activation energy as ~22 meV, close to the thermal energy at ambient (~25 meV) which confirms the fact that the conductivity is governed by the thermal excitation of bound holes [23]. The Ga-doped SnO_2 layers as grown by reactive RF magnetron sputtering process onto Si presented the following parameters: a resistivity, mobility, and a carrier density of 2.8 mΩxcm, 228 cm^2/Vs, and 9x10^{18} cm^{-3}, respectively [43].

Effect of light on I-V characteristics

Effect of light on I-V characteristics of Indium doped (4, 6 and 8 % on SnO_2) thin layer based junction diode at room temperature is evidenced. The measuring setup and the Ag/SnO_2:In/Si/Au MOS junction structure arrangement is drawn in Figure 6. The semilog plotting of current–voltage characteristics of the prepared Al/SnO_2:In/Si/Al diode are studied under dark within the bias voltage (-2,+2) V range between, as shown in Figure 7. A rectifying ratio (RR) is illustrated by two branches that are drawn along the reverse and forward bias voltage bands. RR is the lowest for In 8% doped SnO_2 based diode.

The highest values of current occurred at 2V are 2.19 mA (4%), 1.54 mA (6%), and 1.45 mA (8%). Inside forward voltage around 0-1V band, a straight-line part of I-V curve obeying to V>3kT/q condition postulated by thermionic emission model is observed. Such portion of curve confirms the value of ideality factor greater than one. Using a (dlnI/dV) function, the values of n and I_0 are easily extracted for 4, 6, and 8 % SnO_2 based diode in dark-illumination conditions.

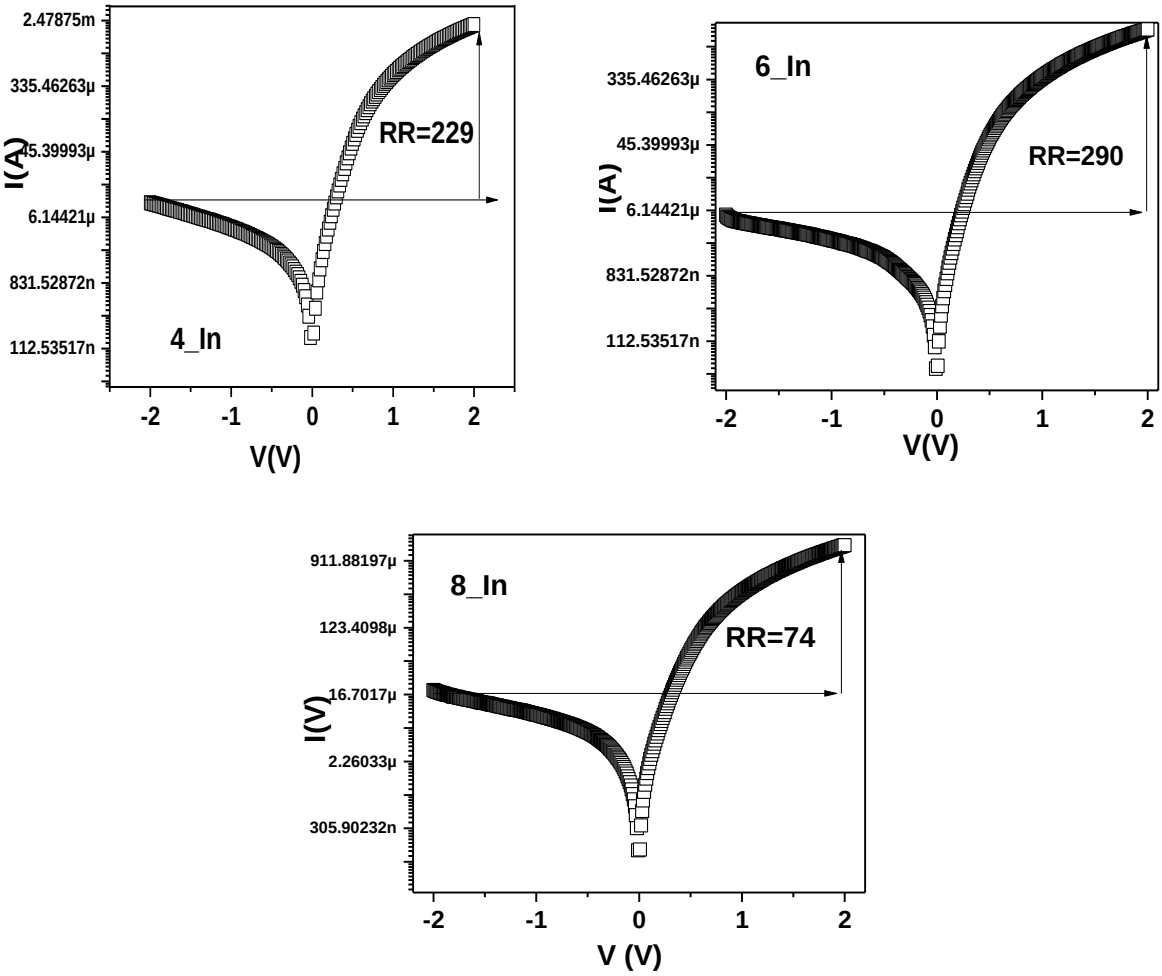

Figure 7: The semi-log diode current versus voltage of the Ag/SnO_2: In/Si/Au junction in dark(RR).

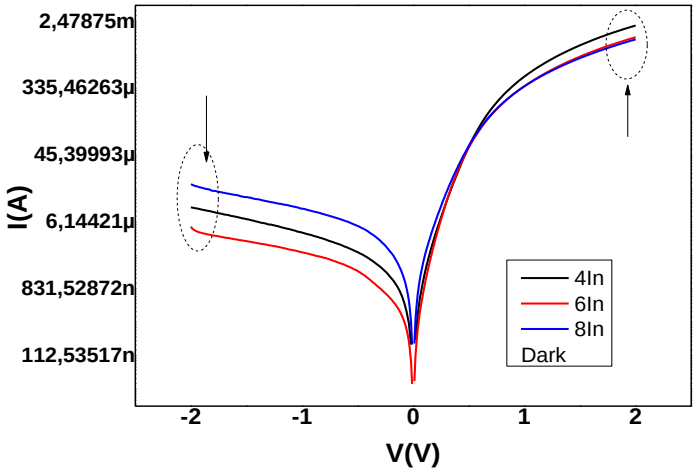

Figure 8: Effect of In-doping level on I-V curves in dark conditions.

Table 5: Ideality factor (n) and saturation current (I_0) of diode based In-doped SnO_2 layers

Ideality factor (I_0 value)			
Light Intensity (mW/cm^2)	**In (%)**		
	4	**6**	**8**
Dark	4.6 (830 nA)	2.8(180nA)	4.3 (1μA)
20	3.4 (215nA)	4.2 (393 nA)	4.55(1.1μA)
40	3.5(231nA)	4.2(400nA)	4.4(1μA)
60	3.5(231nA)	4.1(400nA)	4.38(1μA)
80	3.6(266nA)	4.1(397nA)	4.34(1μA)
100	3.7(393nA)	4.2(465nA)	4.26(0.9μA)

Table 6: Photocurrent I_{ph} , in dark at -2V, I= (3.8μA, %4In), (5.4 μA, %6In), and (17.9 μA, %8In)

Iph (μA)			
Light Intensity (mW/cm^2)	**In 4%**	**In 6%**	**In 8%**
20	5.6	7.4	9.1
40	12.2	9.9	10.1
60	15.2	15.8	16.1
80	21.7	19.4	19.8
100	35.2	25.3	32.2

Table 5 summarizes ideality factor (n) and saturation current (I_0) of diode based (4%-8%) In-doped SnO_2 layers. Effect of In-doping level is evidenced in Figure 8 when device is kept in dark. Arrows indicate effect of In-doping level on I-V values at -2 V and +2 V values. Figure 9 displays the I-V characteristics under illumination showing the variation of photocurrent. The ideality factor (n) of the diode at T=300 K is then expressed as follow [44-45]:

$$n = \frac{q}{kT}\left(\frac{dv}{d\ln(I)}\right) \quad (5)$$

Where, dln(I)/dV signifies the slope of straight part of the forward curve I-V, as seen in Figure 7.

The slope is 0.53 and n=38.67/ slope. At ambient q/kT=38.67 and kT/q=0.02586V. A value of ideality factor of 3 indicating the strong effect of the series resistance in the linear region is occurred. Furthermore, effect of In-doping level is evidenced as portrayed in Figure 10 when device is kept in 100 mW/cm^2 condition. Arrows indicate the effect of In-doping level on I-V values at -2 V and +2 V values. Light intensity decreases the ideality factor (n) and the saturation current I_0 values for 4% In-doped SnO_2. However, illumination intensity increases both n and I_0 values to two times approximately for 6%In doped SnO_2, as listed in Table 6, while a slight shift is observed for 8 In-doped case. It is reported previously that n swept within 2.75-3.58 range and I_0 is about 161-244 nA for p-SnO/n-SnO_2 p-n junction diodes and SnO_2/Ag contact [11]. Diodes display a reverse saturation current of 137 nA and 164 nA by a conventional method

recording (I_f /I_r) ratio of 2 x10^5 and 10.2 at 1V for two fabricated devices. The exponential profile of the forward current-voltage characteristics depends strongly on the property of active material used for heterojunction. It is given in terms of voltage and temperature as follows [46-47]:

$$I = I_0 \left[\exp\left(\frac{qv}{nkT}\right) - 1\right] \quad (6)$$

The reverse saturation current is I_0, can be calculated by extrapolating the linear portion of the semi-log I-V curve as previously expressed [10]. Effective diode area is A=8x10^{-3} cm^2, and the Richardson constant is A* (112 A/cm^2 K^2 for n-type Si) [44-45]. The linear fitting reveals that the saturation current I_0 is determined. Figure 8 illustrates the I-V characteristics for 4, 6, and 8 In-doping under light conditions of 20-100 mW/cm^2. Figure 8 demonstrates how the transport of photogenerated holes inside the diode causes the current to grow with voltage in the reverse voltage region. The photosensitivity (I_ph-I_{dark})/I_{dark} is then calculated at 100 mW/cm^2, and the open circuit voltage V_{oc} is approximately of 40 mV and very small for other light levels as seen in I-V characteristics for 8 %In case, and then V_{oc} is about 0.02 V, is retrieved. According to Ben Haj Othmen *et al.* [3], SnO_2 diode has an ideality factor of 2.95, and iron doping may climb it to 5.45. Likewise, it was stated that while the height barrier remained nearly unchanged with Fe doping, the saturation current and series resistance rose. It is showed that two branches of I-V characteristics are plotted showing an effect of light within the reverse bias voltage, as seen in Figure 9. Likewise, the semilog I-V curve of 4 %In doped SnO_2 demonstrates obviously that exposure to light increased the forward bias voltage. Hence, when V=-2V, a photocurrent (I_{ph}) parameter is derived as I_{ph}=I_{ill}-I_{dark}. In addition, the semilog I-V curve of 6% In-doped SnO_2 clearly shows an increase in forward bias voltage due to the film being exposed to light. Obtained values are listed in Table 6. The SnO_2/FTO current by PLD technique rises nonlinearly for all the voltage values and demonstrates the rectification behavior, as previously reported [26]. For the terminal voltage of 0.6 V, the computed intrinsic voltage across diodes 1 and 2 is found to be 0.346 V and 0.46 V, respectively. The parasitic series resistance measurements for diodes 1 and 2 are 8 KΩ and 5 KΩ, respectively, as cited by Eqbal *et al.* [11]. The electrons at low illuminations are able to overcome the lower barriers because the current transport across the diode interface is generated with a light level, so the current transport will be predominated by the current flowing through the patches with lower BH and a bigger ideality factor. More and more electrons are able to cross the greater barrier as the illumination intensity is increased. The I-V curves are shown for Au contacts on boron-doped diamond and in contacts on SnO_2. These data demonstrate not only that the contacts between the metal electrode and the semiconductor are always ohmic, but also that when PO increases, SnO_2 conductivity falls, meaning that the Fermi level of SnO_2 finally leaves the conduction band as reported by Xue *et al.* [19].

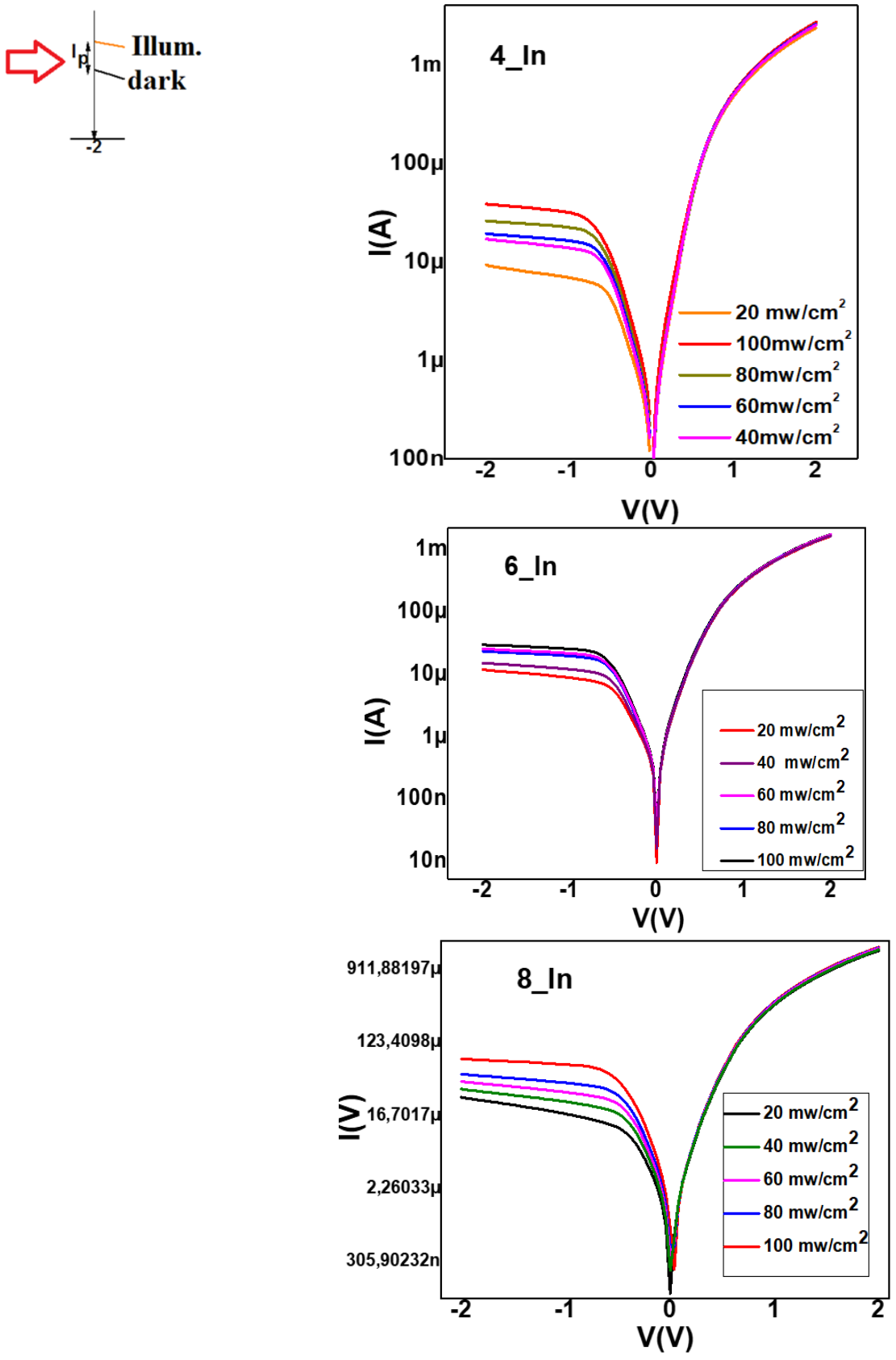

Figure 9: The current-voltage characteristics I-V curves of Ag/SnO_2: In/Si/Au diode in illumination.

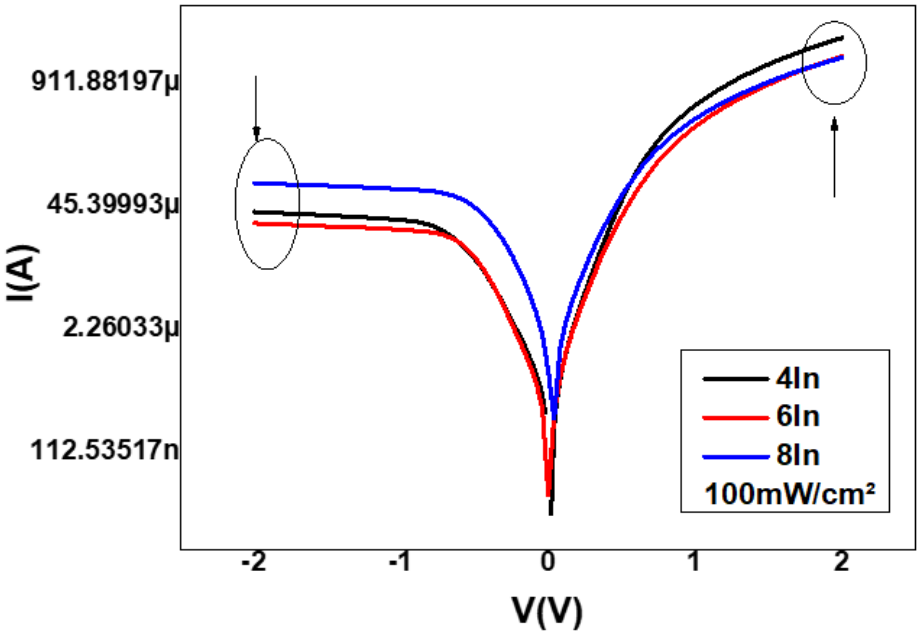

Figure 10: Effect of In-doping level on I-V curves in 100 mW/cm^2 conditions.

Furthermore, more details are introduced in this study, like effect of In-doping level is well evidenced in Figures 8 and 10 both in dark and illumination conditions. Therefore, the current is influenced by In-doping level into SnO_2 lattice at -2V, it is found to be ~17 µA, 6.2 µA, and 8µA for 8%, 6%, and 4% In-doping, respectively, in dark condition. However under light within the reverse voltage range, radiation effect is very important on the current as a result of light intensity. It is revealed that top <100 µA is recorded for 4 and 6% In-doping at 100 mw/cm^2 and increases to 120 µA for 8%In, as seen in Figure 8. Dissimilar trends are observed within forward voltage, current reaches 4% (>1 mA), 6% (~1 mA), and 8%In (950 µA) approximately for all illumination levels. The 8 %In increases current as seen in (-2 V,0 V) reverse voltage range but 4 %In rises current in forward voltage range in particular curved part of I-V characteristics. Recorded values of current (µA) at -2 V are as follows: 9.549 (4 %In), 5.35491 (6 %In), and 19.043 (8 %In). But in forward voltage, results are found to be 2150 (4 %In), 485. 398 (6 %In), and 15.786 (8 %In). The results of this study reveal two different sets of values. Under light, devices present: 38.6521, 29.3277, and 78.1644 µA for 4, 6, and 8 In %, respectively, in reverse, whereas 2700, 1700, and 1600 µA are confirmed in forward biasing, as demonstrated in Figure 9. Prepared by the spray deposition route, Al/SnO_2/p-Si (1 1 1) Schottky diodes demonstrates an ideality factor of 1.9-2.6 as a result of substrate temperature [48]. Altındal reported that n of diode is increasing roughly (2.6 to 7) with temperature lowering (350-80 K). Such values reveal the trap-assisted tunneling and the thermionic emission as the current transport mechanism [49]. The Al/rGO-SnO2/ITO SBD device demonstrates a saturation current of 11-68 µA, as previously reported [50].

Conclusion

In-doped SnO_2 thin films and their properties are successfully fabricated and investigated. Besides, I-V measurements of Ag/SnO_2/nSi/Au heterojunction are investigated under dark and light conditions. Tetragonal crystal structure along (200) orientation is revealed by X-ray analysis. Strong transparency of layers is recorded in particular for 4%In case within visible band. Besides, the highest values of refractive index are recorded for 4%In-doped SnO_2 film. Nanosphere and nanohexagon forms with diverse diameters and configurations are

observed by AFM analysis. Electrical conductivity of In-doped SnO_2 layers in terms of 1000/T is studied and discussed. When n is around 3 higher than unity, this heterojunction displays a non-ideal behavior. The rectification factor and saturation current are measured respectively. Effect of both dark and light on electrical parameters as a result of In-doping amount is well studied and well discussed. Such results allow to our device the photodiode applications.

Acknowledgments

This work is included in the **PRFU2022**project under contract number **B00L02UN310220220001**Oran University of sciences and technology USTO-MB.

Funding

The authors declare that no funding was received for this work.

Data availability

All data generated or analyzed during this study are included in this published article.

Conflict of Interest

The authors declare that they have no conflict of interest. They also declare that they have no known competing financial interests or personal relationships that could have appeared to influence the work reported in this study.

Orcid

Mostefa Benhaliliba: 0000-0001-6507-3663

Reference

[1]. M. Benhaliliba, C. Benouis, F. Yakuphanoglu, A. Tiburcio-Silver, C. Aydin, S. Hamzaoui, Z. Mouffak, Detailed investigation of submicrometer-sized grains of chemically sprayed (Sn1− xAlx, O2)(0≤ x≤ 0.085) thin films, *Journal of Alloys and Compounds*, **2012**, *527*, 40-47. [Crossref], [Google Scholar], [Publisher]

[2]. C. Benouis, M. Benhaliliba, Z. Mouffak, A. Avila-Garcia, A. Tiburcio-Silver, M.O. Lopez, R.R. Trujillo, Y. Ocak, The low resistive and transparent Al-doped SnO_2 films: p-type conductivity, nanostructures and photoluminescence, *Journal of Alloys and Compounds*, **2014**, *603*, 213-223. [Crossref], [Google Scholar], [Publisher]

[3]. W.B.H. Othmen, Z.B. Hamed, B. Sieber, A. Addad, H. Elhouichet, R. Boukherroub, Structural and optical characterization of p-type highly Fe-doped SnO_2 thin films and tunneling transport on SnO_2: Fe/p-Si heterojunction, *Applied Surface Science*, **2018**, *434*, 879-890. [Crossref], [Google Scholar], [Publisher]

[4]. S. Caliskan, G.S. Han, C.Y. Cheng, J.Y. Hong, J.K. Lee, Sequential coating of Sb-doped SnO_2 nanowire for photoelectrochemical cells of panchromatic light absorption and low thermalization loss, *Journal of Power Sources*, **2023**, *570*, 232989. [Crossref], [Google Scholar], [Publisher]

[5]. J. Peng, X. He, C. Shi, J. Leng, F. Lin, F. Liu, H. Zhang, W. Shi, Investigation of graphene supported terahertz elliptical metamaterials, *Physica E: Low-Dimensional Systems and Nanostructures*, **2020**, *124*, 114309. [Crossref], [Google Scholar], [Publisher]

[6]. S.H. Park, Y.K. Oh, Y.J. Lim, C. Shaozheng, S.J. Lee, H.K. Kim, Thermally stable and transparent F-doped SnO_2 (FTO)/Ag/FTO films for transparent thin film heaters used in automobiles, *Ceramics International*, **2023**, *49*, 2419-2426. [Crossref], [Google Scholar], [Publisher]

[7]. C. Ghica, C.G. Mihalcea, C.E. Simion, I.D. Vlaicu, D. Ghica, I.V. Dinu, O.G. Florea, A. Stanoiu, Influence of relative humidity on CO_2 interaction mechanism for Gd-doped SnO_2 with respect to pure SnO_2 and Gd_2O_3, *Sensors and*

Actuators B: Chemical, **2022**, *368*, 132130. [Crossref], [Google Scholar], [Publisher]

[8]. M. Tian, J. Ren, C. Yin, J. Zhou, S. Zhang, Z. Zhang, Multilayer porous Pd-doped SnO_2 thin film: preparation and H2 sensing performance, *Ceramics International*, **2021**, *47*, 28429-28436. [Crossref], [Google Scholar], [Publisher]

[9]. J. Dong, T. Shao, F. Zhang, First-principle study of CO sensing properties on Pt-doped SnO_2 (1 1 0) surface with oxygen defect, *Chemical Physics*, **2023**, *565*, 111739. [Crossref], [Google Scholar], [Publisher]

[10]. S. Yu, L. Yang, Y. Li, X. Qi, X. Wei, J. Zhong, Preferred orientation growth and size tuning of colloidal SnO_2 nanocrystals through Gd^{3+} doping, *Journal of Crystal Growth*, **2013**, *367*, 62-67. [Crossref], [Google Scholar], [Publisher]

[11]. E. Eqbal, R. Raphael, K. Saji, E. Anila, Fabrication of p-SnO/n-SnO_2 transparent pn junction diode by spray pyrolysis and extraction of device's intrinsic parameters, *Materials Letters*, **2019**, *247*, 211-214. [Crossref], [Google Scholar], [Publisher]

[12]. D. Xing, W. Pan, Z. Xie, Q.-S. Jiang, Y. Wu, W. Xun, Y. Lin, X. Yang, Y. Zhang, B. Lin, Improving photovoltaic performance of dye-sensitized solar cells by doping SnO2 compact layer with potassium, *Materials Letters*, **2022**, *327*, 133079. [Crossref], [Google Scholar], [Publisher]

[13]. P. He, H. Fu, Y. Gong, J. Chen, X. Yang, D. Han, S. Xiong, S. Li, X. An, SnO_2@ ZnS core-shell hollow spheres with enhanced room-temperature gas-sensing performance, *Sensors and Actuators B: Chemical*, **2023**, *388*, 133809. [Crossref], [Google Scholar], [Publisher]

[14]. A.P. Caricato, A. Luches, R. Rella, Nanoparticle thin films for gas sensors prepared by matrix assisted pulsed laser evaporation, *Sensors*, **2009**, *9*, 2682-2696. [Crossref], [Google Scholar], [Publisher]

[15]. R. Presley, C. Munsee, C. Park, D. Hong, J. Wager, D. Keszler, Tin oxide transparent thin-film transistors, *Journal of Physics D: Applied Physics*, **2004**, *37*, 2810. [Crossref], [Google Scholar], [Publisher]

[16]. S.H. Lee, D.M. Hoffman, A.J. Jacobson, T.R. Lee, Transparent, homogeneous tin oxide (SnO_2) thin films containing SnO_2-coated gold nanoparticles, *Chemistry of Materials*, **2013**, *25*, 4697-4702. [Crossref], [Google Scholar], [Publisher]

[17]. K. Ozel, A. Atilgan, N.E. Koksal, A. Yildiz, A route towards enhanced UV photo-response characteristics of SnO_2/p-Si based heterostructures by hydrothermally grown nanorods, *Journal of Alloys and Compounds*, **2020**, *849*, 156628. [Crossref], [Google Scholar], [Publisher]

[18].S. Laghrib, M. Benhaliliba, H. Adnani, D. Abdi, Wide bandgap Indium-doped SnO_2 semiconductor prepared by sol-gel route: Multilayer fabrication and Low resistivity for solar cell application, *Journal of Sol-Gel Science and Technology*, **2023**, *106*, 530-544. [Crossref], [Google Scholar], [Publisher]

[19]. J. Xue, K. Liu, B. Dai, B. Liu, L. Yang, J. Han, G. Gao, X. Zhang, J. Zhu, Heterointerface-engineered type II SnO_2/boron-doped diamond heterojunction photodiodes with diverse diode characteristics and binary photoresponse, *Materials Chemistry and Physics*, **2022**, *292*, 126801. [Crossref], [Google Scholar], [Publisher]

[20]. H.S. Akkera, Y. Kumar, M.D. Kumar, G.S. Reddy, B.R. Kumar, U.M. Pasha, Y. Bitla, V. Ganesh, Structural, electrical, and optical properties of rare-earth Sm^{3+} doped SnO_2 transparent conducting oxide thin films for optoelectronic device applications: Synthesized by the spin coating method, *Optical Materials*, **2022**, *133*, 112993. [Crossref], [Google Scholar], [Publisher]

[21]. M. Panday, G.K. Upadhyay, L. Purohit, Sb incorporated SnO_2 nanostructured thin films for CO_2 gas sensing and humidity sensing applications, *Journal of Alloys and Compounds*,

2022, *904*, 164053. [Crossref], [Google Scholar], [Publisher]

[22]. D.A. Aldemir, M. Benhaliliba, C. Benouis, Photodiode based on Al-doped SnO_2: Fabrication, current-voltage and capacitance-conductance-voltage measurements, *Optik*, **2020**, *222*, 165487. [Crossref], [Google Scholar], [Publisher]

[23]. H.P. Dang, Q.H. Luc, T. Le, The influence of deposition temperature and annealing temperature on Ga-doped SnO_2 films prepared by direct current magnetron sputtering, *Journal of Alloys and Compounds*, **2016**, *687*, 1012-1020. [Crossref], [Google Scholar], [Publisher]

[24]. H.W. Kim, S.H. Shim, Ch. Lee,SnO2 microparticles by thermal evaporation and their properties, *Ceramics International* , **2006**, 32, 8, 943-946. [Crossref], [Google Scholar], [Publisher]

[25]. S. Chayoukhi, B. Gassoumi, H. Dhifelaoui, N. Boucherou, A. Boukhachem, M. Amlouk, A. Zghal, Structural, optical and mechanical investigations on pure and Co-doped SnO_2 thin films samples, *Inorganic Chemistry Communications*, **2023**, *149*, 110391. [Crossref], [Google Scholar], [Publisher]

[26]. R. Kajal, B. Kataria, K. Asokan, D. Mohan, Effects of gamma radiation on structural, optical, and electrical properties of SnO_2 thin films, *Applied Surface Science Advances*, **2023**, *15*, 100406. [Crossref], [Google Scholar], [Publisher]

[27]. T. Boucherka, M. Touati, A. Berbadj, N. Brihi, Al^{3+} doping induced changes of structural, morphology, photoluminescence, optical and electrical properties of SnO_2 thin films as alternative TCO for optoelectronic applications, *Ceramics International*, **2023**, *49*, 5728-5737. [Crossref], [Google Scholar], [Publisher]

[28]. S. Yadav, K. Yadav, R. Dhar, D. Mohan, Synthesis and characterization of thermally evaporated Er-doped SnO_2 thin films for photonic applications, *Micro and Nanostructures*, **2023**, *174*, 207493. [Crossref], [Google Scholar], [Publisher]

[29]. Y. Wang, N. Su, J.Liu, Y.Lin, Enhanced visible-light photocatalytic properties of SnO_2 quantum dots by niobium modification, *Result in Physis*, 2022, 37, 105515. [Crossref], [Google Scholar], [Publisher]

[30]. J. Wellings, N. Chaure, S. Heavens, I. Dharmadasa, Growth and characterisation of electrodeposited ZnO thin films, *Thin solid films*, **2008**, *516*, 3893-3898. [Crossref], [Google Scholar], [Publisher]

[31]. N. Kamarulzaman, N.D.A. Aziz, M.F. Kasim, N.F. Chayed, R.H.Y. Subban, N. Badar, Anomalies in wide band gap SnO_2 nanostructures, *Journal of Solid State Chemistry*, **2019**, *277*, 271-280. [Crossref], [Google Scholar], [Publisher]

[32]. D. Mohanta, K. Barman, S. Jasimuddin, M. Ahmaruzzaman, MnO doped SnO_2 nanocatalysts: Activation of wide band gap semiconducting nanomaterials towards visible light induced photoelectrocatalytic water oxidation, *Journal of Colloid and Interface Science*, **2017**, *505*, 756-762. [Crossref], [Google Scholar], [Publisher]

[33]. V. Yadav, N. Singh, D. Meena, Investigation of structural and optical properties of pure SnO2, ZnO and SnO_2/ZnO composite nanorods, *Materials Today: Proceedings*, **2022**, *62*, 3368-3375. [Crossref], [Google Scholar], [Publisher]

[34]. K.J. Archana, A.C. Preetha, K. Balasubramanian, Influence of Urbach energy in enhanced photocatalytic activity of Cu doped ZnO nanoparticles, *Optical Materials*, **2022**, *127*, 112245. [Crossref], [Google Scholar], [Publisher]

[35]. L.M. Jose, N.S. George, S.A. Kadam, S. Athira, A. Kripa, A. Aravind, Y.R. Ma, Y.R. Chen, Insight into the adsorption, photocatalytic and magnetic properties of bandgap tailored hydrothermally grown SnO_2:Ni/Cu nanostructures, *Optical Materials*, **2023**, *135*, 113348. [Crossref], [Google Scholar], [Publisher]

[36]. S. Sambasivam, P.S. Maram, C.V.M. Gopi, I.M. Obaidat, Effect of erbium on the structural,

morphological, and optical properties of SnO2 thin films deposited by spray pyrolysis, *Optik*, **2020**, *202*, 163596. [Crossref], [Google Scholar], [Publisher]

[37]. J. Faucheu, K.A. Wood, L.P. Sung, J.W. Martin, Relating gloss loss to topographical features of a PVDF coating, *JCT Research*, **2006**, *3*, 29-39. [Crossref], [Google Scholar], [Publisher]

[38]. H. Alghamdi, O.Z. Farinre, M.L. Kelley, A.J. Biacchi, D. Saha, T. Adel, K. Siebein, A.R.H. Walker, C.A. Hacker, A.F. Rigosi, Experimental spectroscopic data of SnO_2 films and powder, *Data*, **2023**, *8*, 37. [Crossref], [Google Scholar], [Publisher]

[39]. F.A. Rad, J.T. Mehrabad, M.D. Esrafili, A Communal experimental and DFT study on structural and photocatalytic properties of nitrogen-doped TiO_2, *Advanced Journal of Chemistry, Section A*, **2023**, *6*, 244-252. [Crossref], [Google Scholar], [Publisher]

[40]. R.A. Taj-Aldeen, M.B. Alqaraguly, O.H. Salah, A.S. Abdulwahid, T. Hanoon, Z. Abud Alzahraa, A.A. Omran, Enhanced photocatalytic performance of ZnO NPs in the presence of solar light and H_2O_2 for degradation of tetracycline from wastewater: Optimal conditions for green products, *Advanced Journal of Chemistry, Section A*, **2024**, *7*, 396-405. [Crossref], [Google Scholar], [Publisher]

[41]. F.H. Saboor, A. Ataei, Decoration of metal nanoparticles and metal oxide nanoparticles on carbon nanotubes, *Advanced Journal of Chemistry, Section A*, **2024**, *7*, 122. [Crossref], [Google Scholar], [Publisher]

[42]. S. Ilican, Y. Caglar, M. Caglar, F. Yakuphanoglu, Electrical conductivity, optical and structural properties of indium-doped ZnO nanofiber thin film deposited by spray pyrolysis method, *Physica E: Low-dimensional Systems and Nanostructures*, **2006**, *35*, 131-138. [Crossref], [Google Scholar], [Publisher]

[43]. T. Yang, X. Qin, H.h. Wang, Q. Jia, R. Yu, B. Wang, J. Wang, K. Ibrahim, X. Jiang, Q. He, Preparation and application in p–n homojunction diode of p-type transparent conducting Ga-doped SnO_2 thin films, *Thin Solid Films*, **2010**, *518*, 5542-5545. [Crossref], [Google Scholar], [Publisher]

[44]. S.M. Sze, Y. Li, K.K. Ng, Physics of semiconductor devices, *John Wiley & Sons*, **2021**. [Google Scholar], [Publisher]

[45]. E.H. Rhoderick, R.H. Williams, Metal-semiconductor contacts, *Clarendon Press Oxford*, **1988**. [Google Scholar], [Publisher]

[46]. M. Benhaliliba, A rectifying Al/ZnO/pSi/Al heterojunction as a photodiode, *Micro and Nanostructures*, **2022**, *163*, 107140. [Crossref], [Google Scholar], [Publisher]

[47]. D.A. Aldemir, M. Benhaliliba, C. Benouis, Photodiode based on Al-doped SnO_2: Fabrication, current-voltage and capacitance-conductance-voltage measurements, *Optik*, **2020**, *222*, 165487. [Crossref], [Google Scholar], [Publisher]

[48]. S. Karadeniz, N. Tuğluoğlu, T. Serin, Substrate temperature dependence of series resistance in Al/SnO_2/p-Si (111) Schottky diodes prepared by spray deposition method, *Applied Surface Science*, **2004**, *233*, 5-13. [Crossref], [Google Scholar], [Publisher]

[49]. Ş. Altındal, S. Karadeniz, N. Tuğluoğlu, A. Tataroğlu, The role of interface states and series resistance on the I–V and C–V characteristics in Al/SnO_2/p-Si Schottky diodes, *Solid-State Electronics*, **2003**, *47*, 1847-1854. [Crossref], [Google Scholar], [Publisher]

[50]. P. Das, B. Pal, M. Das, S. Sil, D. Das, A. Layek, P.P. Ray, Findings of inhomogeneity in barrier height of Schottky junction Al/rGO-SnO_2 having anomaly in theoretical and experimental value of Richardson constant: A Gaussian approach, *Results in Physics*, **2022**, *42*, 105996. [Crossref], [Google Scholar], [Publisher]

[51]. S. Gürakar, T. Serin, N. Serin, Electrical and microstructural properties of (Cu, Al, In)-doped SnO_2 films deposited by spray pyrolysis,

Advanced Materials Letters, **2014**, *5*. [Crossref], [Google Scholar], [Publisher]

[52]. C. Benouis, M. Benhaliliba, F. Yakuphanoglu, A.T. Silver, M. Aida, A.S. Juarez, Physical properties of ultrasonic sprayed nanosized indium doped SnO_2 films, *Synthetic Metals*, **2011**, *161*, 1509-1516. [Crossref], [Google Scholar], [Publisher]

[53]. M.H. Khatun, R. Amin, M.S. Islam, M.R. Shikder, Structural and magnetic properties of Fe and Ni co-doped SnO_2 nanoparticles prepared by co-precipitation method, Material Research Express, **2024**, 11. [Crossref], [Google Scholar], [Publisher]